NeuroImage 323 (2025) 121582

Contents lists available at ScienceDirect

NeuroImage

journal homepage: www.elsevier.com/locate/ynimg

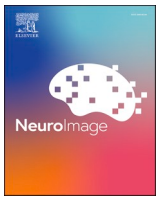

Distinct hippocampus codes for contextual cueing: learning contexts and their predictive associations with targets in visual search

Siyi Chen [a,*], Si Cheng [a], Thomas Geyer [a,b], Hermann J. Müller [a], Zhuanghua Shi [a,b]

[a] Neuro-Cognitive Psychology, Department of Psychology, Ludwig-Maximilians-Universität München, Leopoldstraße 13, 80802 Munich, Germany
[b] NeuroImaging Core Unit Munich (NICUM), Ludwig-Maximilians-Universität München, Nußbaumstraße 7, 80336 Munich, Germany

ARTICLE INFO

Keywords:
Context-based guidance
Context suppression
fMRI
Correlation-based MVPA
DCM

ABSTRACT

Humans can learn to exploit repeated distractor arrangements to optimize attentional selection of targets, producing contextual facilitation. The hippocampus is thought to support context representations acquired from repeatedly searching a given scene layout. However, it remains unclear whether the hippocampus primarily encodes context–target associations, in which the distractor layout directly predicts the target location, or whether it additionally encodes associations among distractors, enabling target prioritization indirectly via context suppression. To examine the neural mechanisms of contextual learning, we combined functional magnetic resonance imaging with a two-phase visual search paradigm: Phase 1 presented predictive (repeated) distractor layouts with consistent target locations, affording contextual cueing; Phase 2 rendered these layouts non-predictive by randomizing target locations, fostering context suppression. Contextual facilitation was compared against a baseline of non-repeated arrangements. We found that both context–target (Phase 1) and distractor–distractor (Phase 2) associations were reliably decoded from the hippocampus using correlation-based multi-voxel pattern analysis. A functional dissociation emerged along the hippocampal axis: anterior and posterior hippocampal regions identified in the whole-brain univariate analyses exhibited relatively greater contributions to Phase 1 context-target and Phase 2 distractor–distractor associations, respectively, indicating their stronger involvement in the corresponding memory representations. Connectivity modeling showed the temporoparietal junction (TPJ) interacted with the hippocampus in different ways depending on context predictivity. These findings indicate anatomically separable hippocampal circuits represent predictive context–target and non-predictive distractor–distractor relations, with their attentional effects gated by the TPJ.

Significance Statement: Although the hippocampus supports the encoding and retrieval of recurrent spatial distractor-target relations in visual search, its distinct roles in representing context-target relations (associating the target location with the configuration of distractors) versus sole-context (distractor-distractor) configurations has not been dissociated. The present study decoded both forms of contextual representation in the hippocampus: the anterior hippocampus preferentially encoded context-target associations, whereas the posterior hippocampus maintained sole-context memory. The signals generated by these distinct hippocampal regions regulate how the target is prioritized for attentional selection, with the temporoparietal junction (TPJ) dynamically adjusting the mode of prioritization in response to the learnt configural structure and how reliably it predicts the target location.

1. Introduction

Statistical regularities – including the spatial relations between targets and distractors – help optimize visual search performance (Awh et al., 2012). Repeated exposure to specific target-distractor configurations, even in abstract arrays, allows these patterns to be encoded in long-term memory, guiding attention to the target when such arrangements are re-encountered – a phenomenon referred to as *contextual cueing* (Chun and Jiang, 1998; Chun and Nakayama, 2000; Goujon et al., 2015). While early studies of contextual cueing focused on scenarios with distractor arrangements that are 100 % predictive of the target location, recent evidence indicates that contextual learning can also occur when only the distractor, but not the target, locations are stable. The latter condition allows learnt distractor configurations to be

* Corresponding author.
E-mail address: Siyi.Chen@psy.lmu.de (S. Chen).

https://doi.org/10.1016/j.neuroimage.2025.121582
Received 15 August 2025; Received in revised form 7 November 2025; Accepted 11 November 2025
Available online 12 November 2025

rejected and thereby raise the attentional priority of the target (Vadillo et al., 2021; Chen et al., 2024). Using functional magnetic resonance imaging (fMRI), the present study investigated the neural mechanisms underlying contextual learning and attentional selection in both predictive and non-predictive search environments.

Within a hierarchical predictive-coding framework (Friston, 2005, 2008), contextual cueing can be explained by higher-level representations generating predictions about expected distractor and target locations and transmitting these signals down the processing hierarchy. This view aligns with observed repetition-suppression effects, where full-repeated displays elicit reduced neural responses across the ventral visual stream, the inferior parietal lobule, and inferior frontal gyrus (Pollmann and Manginelli, 2010; Westerberg et al., 2011; Manginelli et al., 2013). The medial-temporal lobe (MTL; including bilateral hippocampus, parahippocampal, and perirhinal cortices) plays a key role in encoding and retrieving contextual relations among objects (Chun and Phelps, 1999; Greene et al., 2007; Geyer et al., 2012; Manelis and Reder, 2012; Giesbrecht et al., 2013). Other, working-memory-related regions like the intraparietal sulcus (IPS) maintain learnt spatial contexts to guide the allocation of attention (Manginelli et al., 2013). Although traditionally associated with stimulus-driven reorienting (Corbetta and Shulman, 2002), the temporoparietal junction (TPJ), too, is involved in integrating contextual memory with attentional guidance, especially in predictive environments (Geng and Mangun, 2011; Geng and Vossel, 2013; Dugué et al., 2018). There have also been reports of reduced TPJ activity (Shulman et al., 2003, 2007; Wei et al., 2009) reflecting a distractor filtering mechanism that protects goal-driven behavior.

Despite consensus that the hippocampus plays a critical role in encoding and retrieving context-target associations in contextual cueing (e.g., Chun and Phelps, 1999; Greene et al., 2007), no prior work has disentangled the neural representations of (predictive) *context-target* relations from those of (non-predictive) *sole-context* relations. By examining only full-repeated displays with fixed target-distractor relations (against the baseline of novel, non-repeated displays), the extant studies cannot tell whether hippocampal responses reflect memory for the target-in-context or for the contextual structure itself. This raises a fundamental question: does the hippocampus also encode *sole-context* regularities in the absence of target information and, if so, how do these representations differ from those supporting *context-target* associations? Addressing this is crucial for understanding whether the hippocampus acts purely as a target-context binding system that mediates attentional guidance to the target location in fully predictive contexts, or whether it also supports sole-context relational binding mediating target prioritization via distractor suppression in less predictive contexts.

To explore this, we manipulated spatial target-context relationships across two phases, following initial training outside the scanner. In Phase 1, both the distractor and target locations were repeated (*Old-All*), making the target location fully predictive (*context-target learning*). In Phase 2, only the distractor arrangements remained unchanged while target locations varied unpredictably (*Old-D*) (*sole-context testing*). Half of the trials contained no targets. We employed correlation-based multivoxel pattern analysis (MVPA; cf. Haxby et al., 2001) to isolate and compare these memory representations in the hippocampus, allowing these forms of learnt spatial regularity to be directly differentiated. Additionally, we used dynamic causal modeling (DCM) to assess how effective connectivity between the hippocampus and TPJ – two regions linked to contextual memory and attentional control, respectively – is modulated by context predictivity in the presence vs. absence of a target.

2. Materials and methods

2.1. Participants

27 participants (12 females; age: $M = 23.25$ years) took part in the study. All were right-handed and had normal or corrected-to-normal visual acuity. The study was approved by the Ethics Committee of the Department of Psychology, LMU Munich (Project ID 01_Chen_b). All participants provided written informed consent prior to the experiment and received payment for their service.

2.2. Power calculation

To determine the sample size, we performed an a-priori power analysis based on previous studies (Vadillo et al., 2021; Chen et al., 2024). We estimated the least effect size of contextual cueing ($d_z = 1.1$) and context suppression ($d_z = 0.60$). With 85 % power and an alpha level of 0.05, the required sample size was 22 participants to observe a contextual faciliation effect with both full-repeated and distractor-repeated displays. This sample size was also sufficient to detect a contextual facilitation effect in the MTL ($d_z = 0.67$) as reported in previous fMRI studies using ROI analysis (Greene et al., 2007; Preston and Gabrieli, 2008).

2.3. Apparatus

Before the fMRI session, participants received behavioral training outside the scanner to familiarize them with the task. Training took place in a sound-reduced, moderately lit chamber. Stimuli were presented on a 24-in. Samsung SyncMaster screen (1280 × 1024 resolution, 120-Hz refresh rate). Participants viewed the screen at a distance of 60 cm, with heads stabilized using a forehead-and-chin rest and gaze monitored by an EyeLink 1000 eye tracker. During scanning, participants lay down comfortably with their heads in the head coil, cushioned to minimize head movement. Participants viewed the stimuli, projected onto a back projector canvas (diagonal 30 in.) via an adjustable mirror mounted on the head coil, at a viewing distance of 110 cm. The task was presented by an MRI-compatible ProPIXX DLP LED projector (Pixx Technologies Inc, Canada) and responses were collected via a four-button box. Event scheduling and response recording were controlled by customized Matlab codes using the Psychophysics Toolbox (Brainard, 1997; Pelli, 1997).

2.4. Stimuli

The experiment employed variants of the classical "T" vs. "L's" visual-search paradigm: participants searched for a target letter T among 16 distractors L's (randomly rotated by 0°, 90°, 180°, or 270°) and discriminated the orientation of the T (rotated either 90° or 270°) if the target was present (by pressing the left or the right outer buttons on a response pad using their left or right thumbs, respectively) or pressed the inner buttons in case the target was absent, as quickly and accurately as possible (Fig. 1**a**). Distractors appeared at random locations on four concentric (invisible) circles (with radii of 2°, 4°, 6°, and 8° of visual angle, respectively), with the following constraints: all display quadrant contained equal numbers of distractor items (to avoid salient item clusters), and the target appeared only on the second or third ring (to avoid center and outer-edge effects).

2.5. Procedure and design

The MRI session consisted of 20 blocks, each containing 36 trials. The first 10 blocks constituted Phase 1, while the remaining 10 blocks comprised Phase 2. Each trial began with a central fixation marker (0.4° × 0.4° of visual angle) presented for a randomly jittered interval between 1 and 1.3 s, followed by a search display presented for 1 s (Fig. 1**a**). The search display automatically disappeared if a response was made within this period, otherwise it was replaced by a 1-s blank screen. Participants were given up to 1.5 s from display onset to respond; late or empty responses were recorded as misses. After each block, feedback in the form of mean performance accuracy in the just completed block was displayed at the center of the screen.

Three types of display were used: full-repeated displays (Old-All),

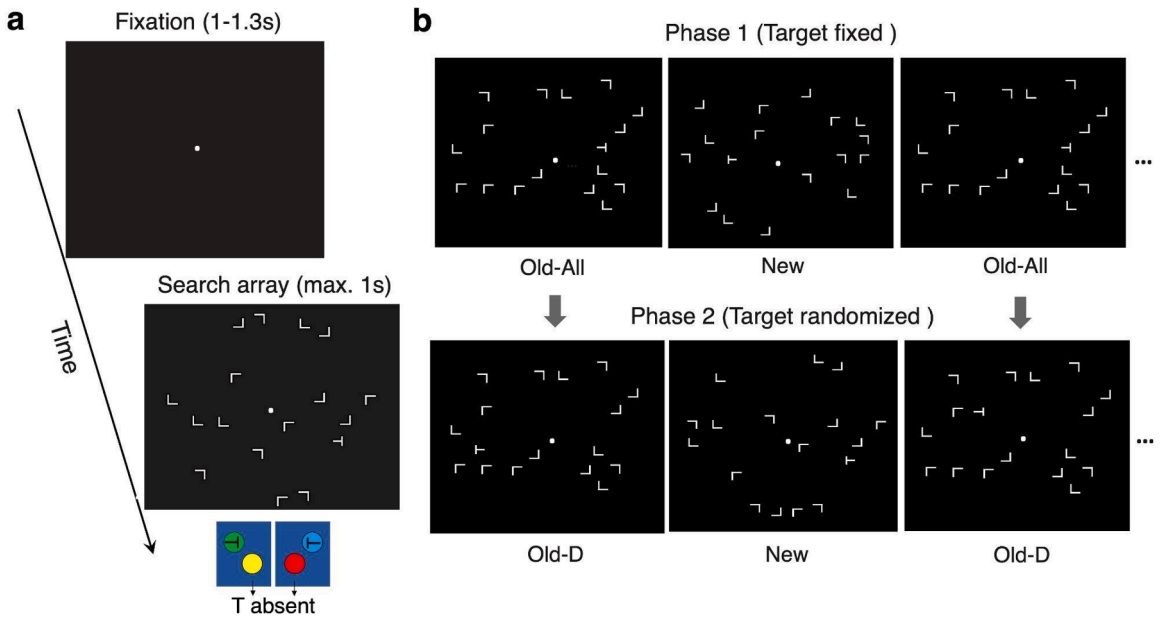

Fig. 1. Schematic illustration of the trial sequence and experimental conditions. (**a**) A trial started with a central fixation marker, followed by a search display that was presented for one second. The task was to find the target T among the L-shaped distractors and discriminate its (left-/right) orientation with the outer buttons (green/blue) of a response pad, as quickly and accurately as possible. If the target T was absent, participants were instructed to randomly press either of the inner buttons (yellow or red). A response made within the display period removed the search display. Participants had to respond within 1.5 s after the onset of the display; otherwise, the response was recorded as 'empty'. The fixation dot was present on the screen throughout the experiment. (**b**) Full-repeated displays (Old-All) with target locations fixed in Phase 1 were transitioned to distractor-repeated displays with target locations randomized (Old-D) in Phase 2, where the old contexts in initially full-repeated displays were rendered non-predictive of the target location despite the distractor configurations remaining the same. In New displays, the distractor arrangements were newly generated in both phases.(For interpretation of the references to color in this figure legend, the reader is referred to the web version of this article.).

where context-target arrangements were fixed; distractor-repeated displays (Old-D), where distractor positions were repeated but the target location varied randomly; and new displays (New), where distractor positions changed on every trial. In Phase 1, there were four distinct full-repeated displays (Fig. 1**b**). Each display had a distinct target location fixed within one particular quadrant relative to an invariant distractor context. Across the four displays, targets appeared in different quadrants to avoid spatial overlapping. During Phase 2, previously predictive contexts (from Phase 1) were rendered non-predictive of the target location, that is, while the distractor arrangement remained constant, the target location became variable; that is, the target appeared at a location that was (pseudo-)randomly selected on a given trial – so that the distractor context could no longer be used as a 'pointer' the target location. To avoid confounding of contextual facilitation by absolute target position learning (Geng and Behrmann, 2005), four distinct target positions were assigned to the old-context condition, and four others to the new-context condition, with the two sets of four fixed target locations changed from Phase 1 to Phase 2. That is, in Phase 2 (in which the distractor context was made non-predictive), the target locations were trial-wise randomized among a set of four distinct positions that had not been occupied by targets in Phase 1, with one set for old-context displays and another set for new-context displays. Selecting a new set of four locations also for new-context displays ensured that the (new-context) baseline condition was comparable between Phases 1 and 2. Within the general constraints just described, the specific displays (i.e., the target locations and distractor arrangements) presented were generated individually for each participant.

Participants were instructed to maintain central fixation during the trial. Compliance was checked by monitoring their eye movements using an eye tracker. The fMRI session was preceded by a behavioral training session and followed by a recognition-memory test (administered outside the scanner). In the post-test, participants were shown 16 trials: eight displays with old contexts (four with target locations from Phase 1 and four with target locations from Phase 2), randomly interspersed with eight newly generated displays. Participants had to classify a given display as "old" or "new" (by pressing the left or the right arrow key), that is: as already seen during the search task or as not seen before.

2.6. *Data acquisition and preprocessing*

The study was conducted at the Neuroimaging Core Unit Munich (NICUM) at LMU Munich on a 3T MRI scanner (Siemens Magnetom Prisma). Functional images were obtained using a multiband accelerated echo-planar imaging (EPI) sequence (TR: 1000 ms; TE: 30 ms; flip angle: 45°; interleaved slice order), permitting us to present the displays relatively fast while controlling eye movements using an MR-compatible EyeLink system. Each volume consisted of 48 transverse slices (field of view: 210 mm; matrix: 70 × 70 pixels; 3-mm isometric voxels; inter-slice gap: 0.3 mm). For co-registration, an additional high-resolution T1-weighted image of the whole brain was acquired prior to the experimental runs using an MPRAGE sequence (TR: 2500 ms; TE: 2.22 ms; 208 transverse slices; matrix: 256 × 256; 0.8-mm isometric voxels).

The analyses were performed with SPM12. The functional images were first preprocessed with realignment, re-slicing, and slice-time correction. Then, head movement was corrected using affine transformation in a two-pass procedure, aligning individual functional images to their mean image using second-degree B-spline interpolation. No participants exceeded the exclusion criteria (translation > 3 mm or rotations $> 3°$). Mean images were then spatially normalized to the 3-mm standard Montreal Neurological Institute (MNI) space using the unified segmentation approach, and the resulting deformation fields were applied to all functional images. The normalized fMRI images were then smoothed with a 6-mm full-width-at-half-maximum (FWHM) Gaussian kernel to improve the signal-to-noise ratio and compensate for residual anatomical variations.

2.7. Behavioral data analysis

Trials with response errors or with extreme reaction times (RTs), defined as below 200 ms or above 2.5 standard deviations from an individual's average RT per condition, were excluded from RT analysis (2.4 %). Since generalized linear mixed-effects models (GLMMs) provide a flexible framework for modeling non-normally distributed data and account for subject-level variability, we applied GLMMs to the raw RT data. A Gamma distribution with a log link function was used, appropriate for the positively skewed RT data. For the training session conducted outside the scanner, the model included the fixed effects of **Block** (B; modeled as log-transformed), and **Display** (D; old vs. new). For the **scanning session**, fixed effects included **Block** (log-transformed), **Display** (old vs. new), **Target presence** (T; present vs. absent), and **Phase** (P; Phase 1 vs. Phase 2). Participant was included as a random factor with a random intercept and slopes for conditions to account for individual differences in baseline response times and in the effects of different experimental conditions (see also Chen et al., 2024). All GLMMs were fitted using the **glmmTMB** package (Brooks et al., 2017) in R. Assuming no RT difference between different types of display in the first block, but gradual development of contextual-facilitation effects across the blocks (cf. Chun and Jiang, 1998), we defined the model for the training session as follows:

$$RT_{ij} = b_0 + [b_1 + b_2 D_{old}]log(B_i) + u_j + v_{1j}log(B_i) + v_{2j}D_i + \epsilon_{ij}$$

where b_0 is the fixed intercept, representing the estimated RT in Block 1, while b_1 captures the overall learning rate and b_2 represents the contextual-facilitation effect for full-repeated relative to new displays. Furthermore, u_j is the participant-level random intercept, while v_{1j} and v_{2j} model individual variation across blocks and displays, respectively.

During scanning, the model incorporated additional factors that allowed us to test additional effects of our experimental manipulations (namely, fixed vs. variable target placements and target-absent vs. target-present trials):

$$RT_{ij} = b_0 + b_1 log(B_i) + b_2 D_{old} + b_3 T_{absent} + (b_4 D_{old} + b_5 T_{absent}) log(B_i) + b_6 D_{old} T_{absent}$$

$$+ b_7 D_{new} T_{present} P + b_8 D_{old} T_{present} P + b_9 D_{new} T_{absent} P + b_{10} D_{old} T_{absent} P$$

$$+ u_j + v_{1j} log(B_i) + v_{2j} T_i + v_{3j} D_i + \epsilon_{ij}$$

In this model, b_0 represents the RT in Block 1 for the baseline condition (New displays, Target present). b_1 reflects context-independent procedural learning (i.e., facilitation in terms of search RT with time on task for new- as well as old-context trials), b_2 represents the main effect of display type (Old vs. New in the presence of the target), while b_3 captures the main effect of target presence in new displays. b_4 and b_5 represent how the learning rate differs by display type and target presence, respectively. b_6 represents their interaction, and b_7 – b_{10} capture three-way interactions involving display type, target presence, and experimental phase, testing whether these effects change between phases. Participant-level random intercepts and slopes (u_j, v_{1j}, v_{2j}, v_{3j}) capture individual differences in baseline RTs and condition effects.

Accuracy was modeled using a GLMM with a binomial distribution and a logit link function, appropriate for binary outcomes (e.g., response correct/incorrect). The model included the same fixed effects as the RT model. Participant was treated as a random effect.

The selected models did not differ significantly from the corresponding full factorial models (all likelihood test $ps > 0.1$). Since our selected models align with the theoretical hypothesis while possessing a simpler structure, we report the results from these models.

2.8. Imaging data

Visual stimulus-onset vectors were defined for the 24 different conditions, that is: 4 Configuration Types (the four repeated context–target pairings in Old-All, the four repeated distractor-only contexts in Old-D, and the four repeated target locations with randomized distractors in New displays) × 2 Target locations (or Phases: Phase 1, Phase 2) × 3 Display Types (Old-present, Old-absent, New-present). Events were convolved with the canonical hemodynamic response function (HRF), and the six head movement parameters were included as nuisance regressors. Finally, each experimental regressor was contrasted against the implicit baseline to generate the first-level contrasts for the subsequent correlation-based MVPA.

We also conducted a separate first-level GLM analysis with a full factorial design: 2 (Phase: Phase 1, Phase 2) × 2 (Display: old, new) × 2 (Target Presence: present, absent). Also, events were convolved with the canonical HRF, and the six head-movement parameters were included as nuisance regressors. The resulting contrast images were entered into a second-level flexible factorial design with "conditions" as within-participant factors and participants as a random factor, implementing a random-effects analysis. We quantified learning by computing two contrasts using planned t-contrasts, familywise error (FWE) corrected at the cluster-level (with voxel-level cut-off of $p < .001$): Old-All vs. New1 for classic context-target learning, restricted to target-present trials; Old-D vs. New2 for sole-context learning, pooling across target-present and target-absent trials. The effect of Target Location (Phase), the effect of Target Presence, and the interaction between Display and Target Presence were also assessed.

2.9. Correlation-based MVPA

To investigate long-term-memory (LTM) representation similarities of the different display types, we conducted *correlation-based* multi-voxel pattern analysis (MVPA) using the Decoding Toolbox (Hebart et al., 2014). ROIs were defined in bilateral hippocampus using the Harvard-Oxford probability atlas (> 30 % voxel probability). We assessed the trial-by-trial activation patterns elicited by each critical image by computing correlations across voxels within the ROI. For each image, the correlation of its activation pattern with itself (averaged within condition) occupied the diagonal elements of the similarity matrix, while correlations between different images were represented in the off-diagonal elements. Specifically, for Old-context displays, we extracted the four repeated-distractor configuration values from the relevant voxels. For New displays, values were computed across random configurations for each of the four target locations. For each of the six conditions (3 Display Types × 2 Phases), correlation distances were computed using Pearson's r as the similarity metric between beta weights. The correlation coefficients were Fisher z-transformed for statistical testing. Accordingly, lower z values indicate greater representational distinctiveness. We performed an rm-ANOVA on the similarity coefficients with the two factors Target location (Fixed vs. Randomized) and Display (Old, New). That is, we first combined the target-present and target-absent trials for Old-context displays and compared the combined score for Old-context displays with New-context displays. Next, we compared Old-All vs. Old-D displays specifically. We expected greater similarity for Old vs. New contexts regardless of Phase because of repeated-context learning, and greater similarity for Old-All vs. Old-D displays because of the randomized target locations in the latter. Particularly, Old-D with target absent should engender higher similarity than Old-D with target present.

2.10. Dynamic causal modeling

We selected the hippocampus and TPJ as ROIs for connectivity analyses, given their respective roles in memory encoding/retrieval and attentional selection. Each ROI was defined as a 6-mm-radius sphere centered on participant-specific local maxima ($p < 0.05$, uncorrected) near group-level peaks. Mean-adjusted data (i.e., first Eigenvariate of the time series) from each participant were extracted from all voxels

within left aHPC, pHPC, and TPJ. Left aHPC coordinates were based on the contrast Old-All vs. New1 (both for target-present conditions), left pHPC on the contrast Old-D vs. New2 (combining both target-present and target-absent conditions), and left TPJ on the interaction contrast Display (Old > New) × Target presence (target present > target absent).

Effective connectivity was assessed using dynamic causal modeling – parametric empirical Bayes (DCM-PEB). First, a full connected bilinear deterministic DCM without centering around the mean (Friston et al., 2003) was estimated for each participant in SPM12 (cf. SPM procedure: spm_dcm_fit). The model included (i) all fixed endogenous connections (matrix A), (ii) all modulatory effects of condition (matrix B), and (iii) experimental inputs (matrix C). Second, PEB modeled group-level effects across all parameters (cf. SPM procedure:spm_dcm_peb), focusing on average connectivity across all participants, taking into account the within-participant variability on the connectivity parameters while ignoring between-participant factors. Bayesian Model Reduction (BMR) was applied to iteratively prune parameters that contributed least to model evidence (cf. SPM procedure:spm_dcm_peb_bmc). BMR has the advantage that any reduced model at the group level can be estimated efficiently without having to re-estimate the reduced models at the single-participant level. Specifically, a greedy search iteratively compared the full model with 256 models where one or more connections with least evidence are pruned and thus disabled, whereas the parameters with the most evidence are kept stable so that the most relevant nested models from the full PEB model are tested (Friston and Penny, 2011; Friston et al., 2016). Next, Bayesian model averaging (BMA) of the parameters across models was applied and used for group inferences (e.g., Penny et al., 2006). Parameters with posterior probability > 0.95 were considered significant.

2.11. Code and data accessibility

The data and key analysis code supporting the study's findings are available at https://gin.g-node.org/siyi.chen/CCfMRI. This study's design and its analysis were not preregistered.

3. Results

3.1. Behavioral data

3.1.1. Training phase

Both the accuracy and RT data showed effective procedural learning and context-dependent learning (Figs. 2**a–b**). On average, participants achieved 92.4 % accuracy for full-repeated displays and 88.5 % for new displays. A GLMM showed that accuracy on new displays increased by 3 % per log(Block) (95 % CI [+2 %, +5 %], $p < .001$), reflecting procedural learning. Importantly, accuracy for full-repeated displays improved by an additional 5.5 % per log(Block) (95 % CI [+4 %, +7 %], $p < .001$), evidencing enhanced context-based learning. RTs were analyzed with a GLMM (Gamma family, log link). The model estimated an initial mean RT of approximately 825 ms. RTs decreased by about 5 % per log(Block) for new displays (95 % CI [–7 %, –3 %], $p < .001$), corresponding to a reduction of roughly 41 ms. For repeated displays, an additional 4 % reduction was observed (95 % CI [–5 %, –3 %], $p < .001$), equivalent to a further 30–35 ms decrease. Together, these results confirm effective contextual learning above and beyond procedural learning before the scanning session.

3.1.2. Scanning phase

The learning effect transferred to the scanner phase (Fig. 2**c–f**). Participants showed 5 % higher accuracy for Old-context compared to New-context displays (88 % vs. 83 %; 95 % CI [+3 %, +7 %], $p < .001$), confirming preserved contextual cueing (Fig. 2c). Responses were generally 9 % more accurate on target-absent than target-present trials (91 % vs. 82 %; 95 % CI [+6 %, +12 %], $p < .001$), and accuracy for target-absent trials improved ~5 % faster per log(Block) (95 % CI [+3

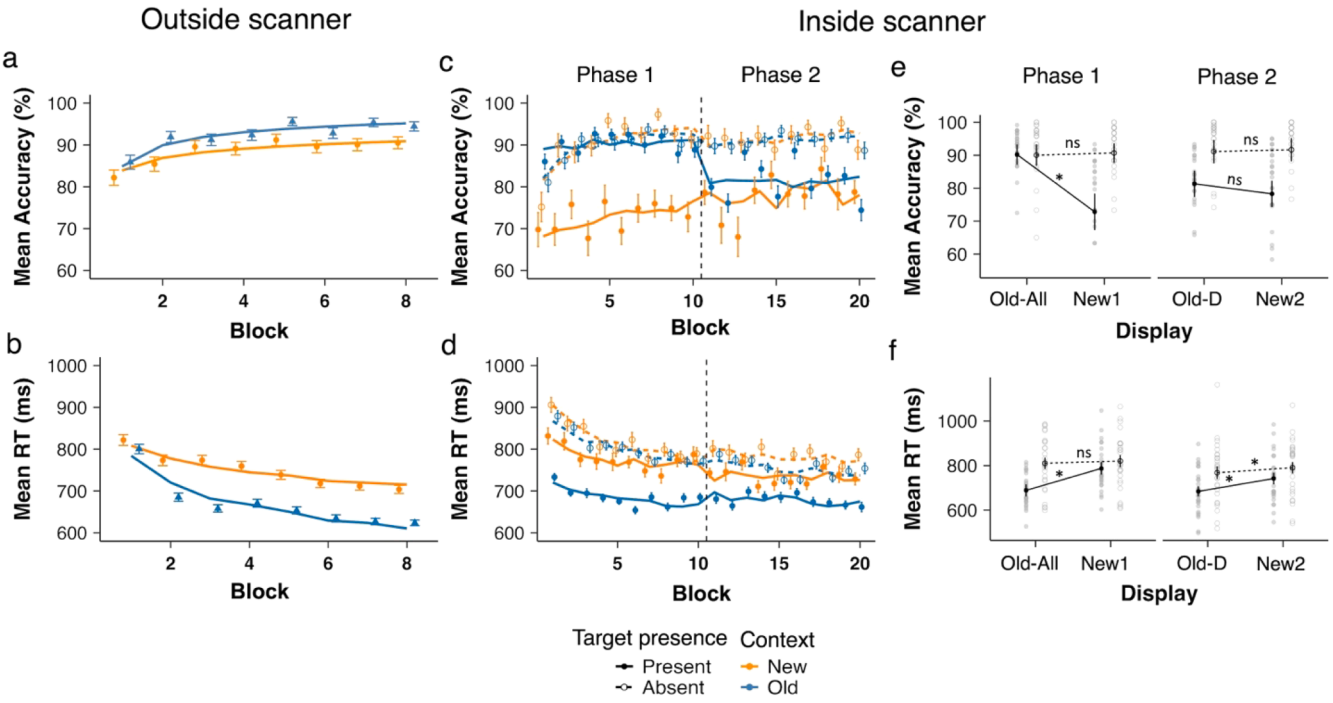

Fig. 2. Behavioral results from the training session (outside the scanner) and the test session (inside the scanner). Panel (**a**) and (**b**) show mean accuracy and RTs, respectively, during the training session (1 block = 4 repetitions, 32 trials), and panels (**c**) and (**d**) depict accuracy and RTs during the test session. Data are plotted as a function of block, separately for Old and New distractor contexts and for target-present and -absent conditions during the test session. Panels (**e**) and (**f**) depict the accuracy and RT data, respectively, averaged per phase. Old contexts are labelled Old-All and the new contexts New1 in Phase 1 with fixed target locations (Block 1–10); and old contexts are labelled Old-D and new contexts New2 in Phase 2 with randomized target locations (Block 11–20). * denotes $p < .01$ and n.s. non-significant.

%, +8 %], $p < .001$), likely reflecting a bias to respond 'target absent' rather than 'target present', as is typically observed in hard search tasks). A significant interaction between Target presence and Display arose because the accuracy difference between target-absent and target-present trials was smaller for Old-context (≈ 5 %) than for New-context displays (≈ 16 %) (95 % CI [–10 %, –7 %], $p < .001$). A further three-way interaction between Phase, Target presence, and Display indicated a selective decline when predictive contexts lost validity. Accuracy dropped by 9 % from Phase 1 to Phase 2 on target-present trials for Old-context displays (95 % CI [–12 %, –7 %], $p < .001$), but showed a 5 % non-significant increase for New-context displays (95 % CI [–1 %, +8 %], $p = .13$). Across both contexts, the phase-related decline was smaller for target-absent than for target-present trials (New-context:6 %, 95 % CI [–10 %, –2 %], $p = .001$; Old-context:5 %, 95 % CI [–8 %, –3 %], $p < .001$). Thus, there was a specific cost (~9 % accuracy loss) when previously predictive contexts (Old-All in Phase 1) became non-predictive (Old-D in Phase 2)—a pattern not observed for new, never-predictive contexts.

The GLMM (Gamma family, log link) on RT data revealed a robust contextual-cueing effect (Fig. 2**d**). Responses were significantly faster for Old-context than New-context displays, with mean RTs being 12 % shorter (95 % CI [–15 %, –10 %], $p < .001$). The average baseline RT for New-context/Target-present trials was approximately 822 ms (95 % CI [783, 863], $p < .001$). RTs decreased by about 3.4 % per log(Block) (95 % CI [–6 %, –1 %], $p = .003$), reflecting continued procedural learning. Learning rates did not differ between Old- and New-context displays (difference = +0.1 %, 95 % CI [–1 %, +1 %], $p = .86$), suggesting retained learning without further enhancement. Target-absent trials were on average 9 % slower than target-present trials (95 % CI [+4 %, +14 %], $p < .001$), but they exhibited a 2.8 % steeper learning slope (95 % CI [–4 %, –2 %], $p < .001$). An interaction between Display type and Target presence showed a greater RT difference between target-absent and target-present trials for Old-context compared with New-context displays, with RTs being 12 % longer in the Old-context/Target-absent condition (95 % CI [+10 %, +14 %], $p < .001$). The three-way interaction among Display, Session, and Target presence indicated a phase-related transition cost. In Session 2, RTs increased by about 3 % for Old-context/Target-present trials (95 % CI [+1 %, +4 %], $p < .001$), but decreased by 2 % for New-context/Target-present trials (95 % CI [–4 %, 0 %], $p = .078$). Thus, consistent with the accuracy results, there was a phase-related transition cost due to the reduced contextual predictivity in Phase 2.

Importantly, direct comparisons between Phases 1 and 2 confirmed the distinct benefits of the learnt contexts (Fig. 2**e–f**). In Phase 1, Old-All displays (predictive contexts) engendered larger performance gains (in both accuracy and RTs) than New displays, but only when the target was present (accuracy difference = 17 %, t (26) = 5.97, $p < .001$, $d_z = 1.15$; RT difference = 99 ms, t (26) = 9.41, $p < 0.001$, $d_z = 1.81$), and not when a target was absent (ts (26) < 1.23, ps > 0.23, d_zs < 0.24). However, even after transitioning to Old-D displays in Phase 2 (in which the target location was no longer fixed), significant RT benefits persisted for Old-D vs. New displays, whether a target was present (58 ms) or absent (23 ms, ts (26) > 2.82, ps ⟨ 0.009, d_zs ⟩ 0.54). This is suggestive of efficient distractor rejection despite the reduced target predictivity.

3.1.3. Recognition results

Participants' explicit recognition performance – their ability to discriminate repeated displays ('signals') from non-repeated ones ('noise') – was assessed by the signal-detection sensitivity parameter *d'* (Green et al., 1966). The mean *d'* score (d' = 0.003) was close to, and not significantly different, from zero, t (26) = 0.03, $p = .98$, $d = 0.006$, suggesting that observers had little (if any) awareness of the repetition of (specific) distractor arrangements.

Overall, the behavioral data indicate that participants successfully acquired the repeated contexts outside the scanner and used this implicit knowledge during Phase 1, with fixed, context-predicted target locations, inside the scanner. Although there was a performance cost when the distractor context was rendered non-predictive of the target location in Phase 2, participants were still able to exploit the contexts to facilitate target detection – evidenced by a persistent performance benefit relative to the new-context baseline, though a lesser benefit compared to the predictive contexts in Phase 1. This reduced facilitation effect with non-predictive contexts cannot reflect contextual guidance (as the acquired 'cues' to the target location were no longer valid), but instead is likely attributable to participants reverting to a less efficient distractor-context suppression strategy to single out the target item (Chen et al., 2024, 2025a, 2025b).

3.2. fMRI data

3.2.1. Correlation-based MVPA

The main goal of the present study was to elucidate the brain regions involved in context-target learning and sole-context (re-)learning, respectively. Based on previous studies (e.g., Chun and Phelps, 1999; Geyer et al., 2012; Manelis and Reder, 2012; Giesbrecht et al., 2013), we expected the hippocampus to contribute to these forms of learning. To differentiate between the two types of contextual learning – context-target association (affording target prioritization via contextual cueing) and distractor-distractor association (affording target prioritization via context suppression) – we applied correlation-based MVPA to hippocampal (HPC) activity patterns (Fig. 3**a**). We performed an rm-ANOVA on the similarity coefficients with the two factors Target location (Fixed vs. Randomized) and Display (Old, New) (Fig. 3**b**). The analysis revealed both main effects to be significant: representational similarity was higher when the target location was fixed vs. randomized, F (1, 26) = 5.40, $p = .028$, $\eta_p^2 = .17$, and markedly higher for Old vs. New displays, F (1, 26) = 245.62, $p < .001$, $\eta_p^2 = .90$. Although the Target location × Display interaction was only marginally significant, F (1, 26) = 3.76, $p = .06$, $\eta_p^2 = .13$, post-hoc testing suggested representational similarity to be higher when the target location was fixed rather than randomized for Old displays, t (26) = 2.73, $p = .01$, $d_z = .53$, but not for New displays, t (26) = 1.33, $p = .19$, $d_z = .26$. Interestingly, this was the case even for Old-absent displays with the exact-same distractor-only arrangements in both phases: for these, too, representational similarity was greater in Phase 1 (Old-All, target-absent) than in Phase 2 (Old-D, target-absent), t (26) = 3.04, $p = .005$, $d_z = 0.59$. Thus, the MVPA results confirm the behavioral findings: the initial (Phase 1) context-target representations in the hippocampus proved quite robust, likely because the distractor-target associations were already well established prior to the scanner session. Notably, even after transitioning to conditions in which the target locations were no longer predictable (in Phase 2), hippocampal patterns continued to represent the distractor-context quite consistently. These findings suggest that hippocampal encoding of spatial context is sustained and remains relatively coherent even when task-relevant target properties become unpredictable.

3.2.2. Whole-brain univariate analysis and ROI selection

We focused on two key contrasts: (1) Old-All vs. New (Phase 1, target-present trials), which aimed to capture regions involved in stable context-target association; (2) Old-D vs. New (Phase 2, target-present and -absent trials), aiming to identify regions involved in processing familiar distractor contexts that afford no reliable prediction of the target location – hypothesized to engage context-suppression mechanisms. The first – Old-All vs. New1 (target-present) display – contrast showed activations in the left anterior hippocampus (aHPC, $x = -30$, $y = -10$, $z = -16$, cluster size = 31 voxels, $T = 3.81$). Additionally, left precuneus, bilateral Angular gyrus, left ACC, left rectal gyrus, left superior medial and frontal gyrus, and left middle temporal gyrus were activated (Fig. 4**a**, Table 1). The second – Old-D vs. New2 display – contrast revealed activations only in the bilateral posterior hippocampus (left pHPC, $x = -21$, $y = -43$, $z = 11$, cluster size = 70 voxels, $T = 3.95$;

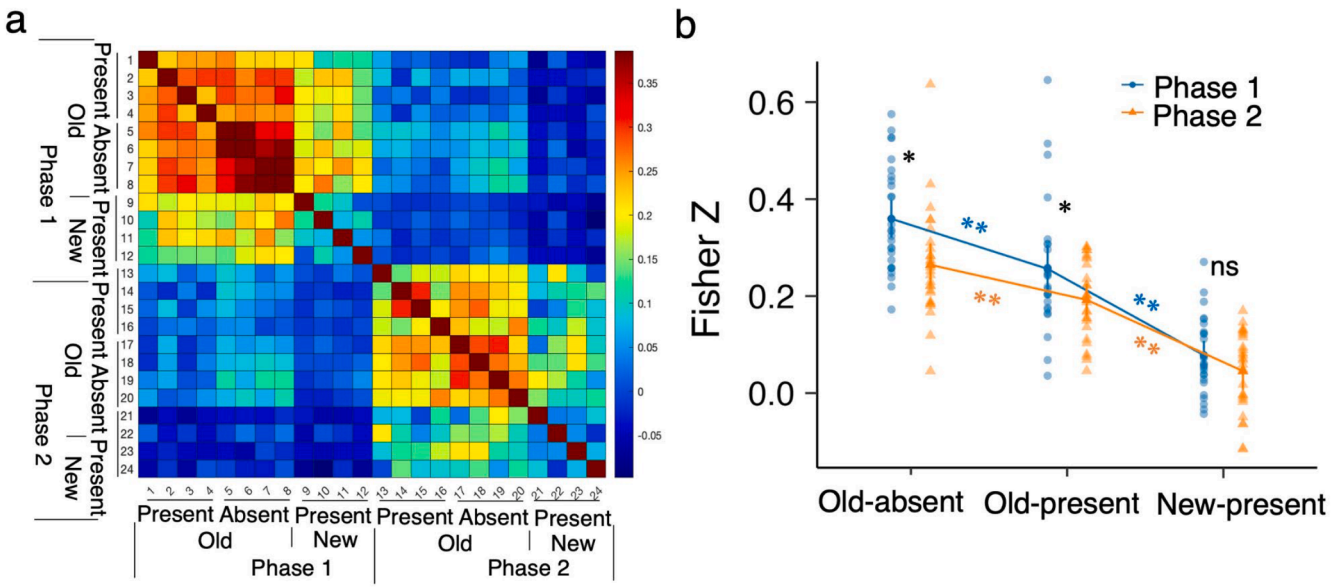

Fig. 3. **a** Similarity matrices in the hippocampus area of correlation-based MVPA. **b** The mean z scores in different conditions based on the similarity matrices in **a**. * denotes $p < .05$, ** $p < .01$, and n.s. non-significant.

right pHPC, $x = 24$, $y = -43$, $z = 11$, cluster size = 67 voxels, $T = 3.92$).

To quantify these effects, beta values were extracted from 3-mm-radius spheres centered on peak hippocampal coordinates (see Fig. 4**a**). In the left aHPC, activation was significantly greater for Old- vs. New-context displays in Phase 1, but only when the target was present ($t(26) = 3.75$, $p < .001$, $d_z = 0.72$); no significant differences were observed between old and new displays when the target was absent in Phase 1 or in Phase 2, whether or not a target was present (*all ps* $> .15$, d_zs < 0.29). In contrast, the bilateral pHPC exhibited greater activation for Old- vs. New-context displays in Phase 2, regardless of target presence (*ts* > 2.22, *ps* $\langle .035$, d_zs $\rangle 0.43$); no significant effects were observed in Phase 1 for the bilateral pHPC signals (*ps* $> .09$, d_zs < 0.34). This pattern suggests a *functional dissociation* along the hippocampal longitudinal axis: the aHPC is more engaged when the distractor context reliably predicts the location of a target that is present in the display, whereas the pHPC is recruited regardless of target presence under conditions of low contextual predictivity.

To pinpoint the regions mediating context effects on attentional target selection, we examined the interaction contrast: (Old > New) × (Target present > Target absent), disregarding Phase in the first instance. This contrast revealed increased activations in the left superior frontal gyrus (SFG), left precuneus, and left angular gyrus within the temporoparietal junction (TPJ), along with decreased activations in the right inferior frontal gyrus (IFG). Beta values extracted from the left TPJ (Fig. 4**a**, Table 1; $x = -39$, $y = -61$, $z = 35$, cluster size = 128 voxels, $T = 4.69$) showed that in *Phase 1*, left TPJ activation was *higher* for Old vs. New contexts when the target was *present,* $t(26) = 4.57$, $p < .001$, $d_z = 0.88$, without a significant difference when the target was absent, $t(26) = -0.44$, $p = .67$, $d_z = -0.08$. In *Phase 2*, by contrast, left TPJ activation was significantly *lower* for Old vs. New contexts when the target was *absent,* $t(26) = -2.36$, $p = .03$, $d_z = -0.45$, with some tendency for activation to be higher for Old contexts when the target was present, $t(26) = 1.85$, $p = .08$, $d_z = 0.36$. This pattern suggests that the left TPJ supports attentional selection of a target embedded within a learnt distractor context especially when the context reliably predicts target location; in contrast, when the target is absent, it helps reduce attentional deployment, especially when the target location is not reliably predicted by the context.

Additional results from the whole-brain univariate analysis are summarized in Fig. 4**b** In both phases, the New vs. Old contrast revealed greater activation across multiple occipital and fusiform regions, including the right fusiform gyrus, bilateral middle occipital gyrus, and, on the left, the inferior occipital gyrus, lingual gyrus, and superior parietal lobule. These activations are consistent with repetition suppression, where repeated stimuli elicit reduced neural responses (Grill-Spector et al., 2006; Summerfield et al., 2008). We also examined Phase effects for Old- and New-context displays separately. The contrast Old-D vs. Old-All – comparing less predictive with fully predictive learnt contexts – revealed significant activations in both the pHPC and caudate, along with bilateral engagement of the posterior medial frontal cortex (pMFC). In Phase 2 (Old-D), previously learned contexts elicited stronger engagement of the hippocampal memory system than in Phase 1 (Old-All), likely because they had lost their predictivity with respect to the target locations. Accordingly, the increased posterior hippocampal activation may reflect the need to re-evaluate memory representations, to reconcile familiar distractor contexts with new and relatively unpredictable target locations. Concurrently, caudate activation may reflect procedural adjustments in response selection when prior learning must be overridden (Packard and Knowlton, 2002; Grahn et al., 2008). Of note, the caudate was also more active for New displays in Phase 2 vs. Phase 1 (New2 > New1), consistent with a role in procedural learning.

3.2.3. DCM-PEB

To further explore the network-level dynamics between memory-related (HPC) and attentional-selection-related (TPJ) regions, we used DCM-PEB to assess effective connectivity between the left aHPC and the left TPJ during Phase 1 (target location fixed), and between the left pHPC and the left TPJ during Phase 2 (target location randomized). Given that only the left aHPC was activated for context–target associations (in Phase 1), and bilateral pHPC for familiar distractor contexts (in Phase 2), we focused on the left hemisphere to facilitate direct comparison of effective connectivity across phases. Therefore, the DCM analyses focused on the phase-specific regions showing significant activation. This approach ensured that connectivity was modeled only among functionally relevant regions identified in each phase. For the right pHPC–left TPJ connectivity in Phase 2, both regions exhibited only negative self-connections and no significant reciprocal influences. As can be seen from Fig. 4**c**, all regions exhibited negative intrinsic (self-) connections (gray) across both phases, suggesting local inhibitory regulation. In addition, in Phase 1, the intrinsic connection from aHPC to TPJ was significant, while there were no significant intrinsic connections between the left pHPC and left TPJ in Phase 2.

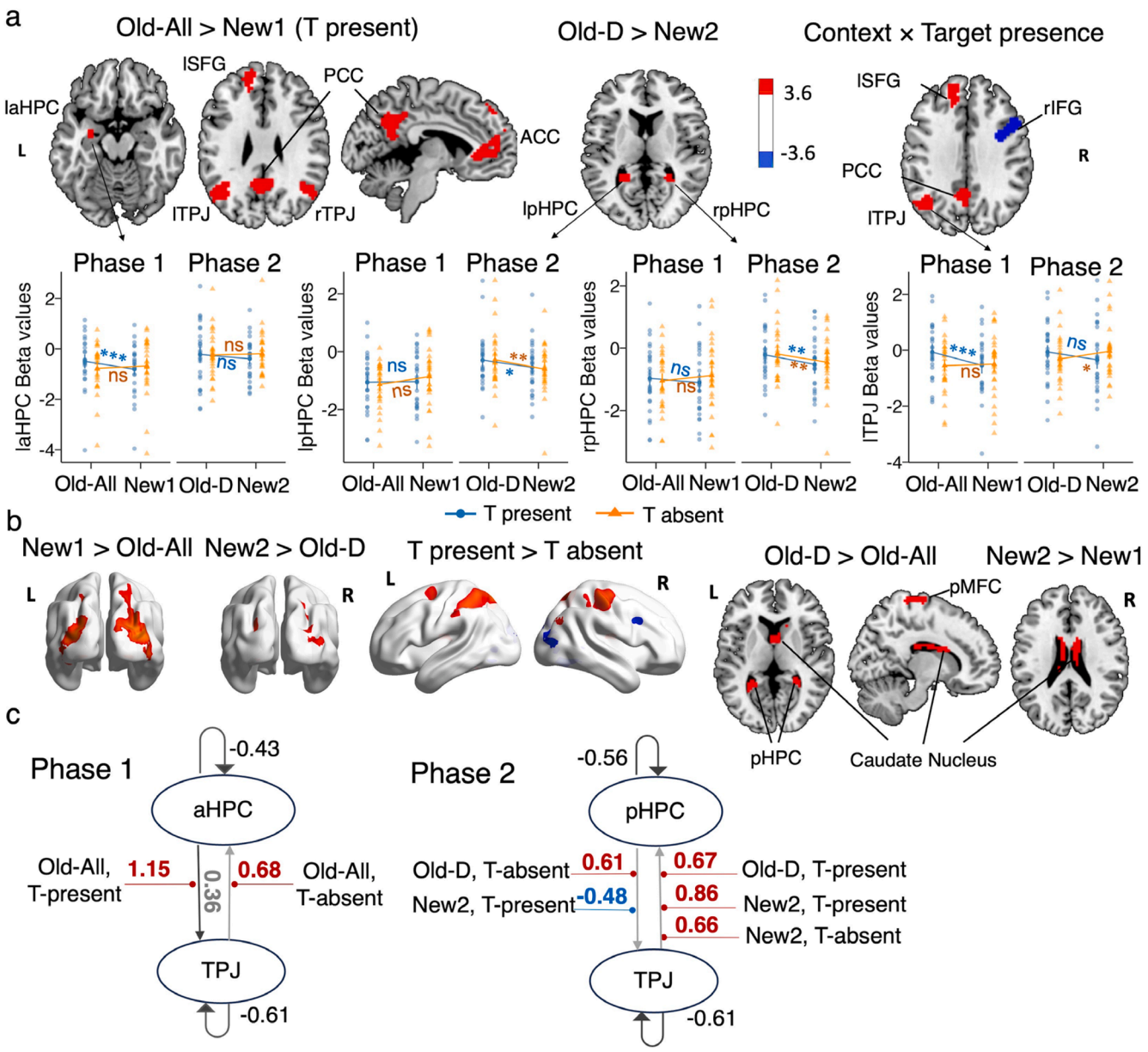

Fig. 4. ROI selection and DCM. (**a**) Whole-brain activation maps showing significant clusters for key contrasts between experimental conditions and corresponding beta estimates comparison across experimental conditions in regions of interest: hippocampus (HPC) and temporo-parietal junction (TPJ). (**b**) Additional whole-brain activation maps showing significant clusters for other contrasts between experimental conditions. (**c**) DCM-PEB results. All connections denote a posterior probability $> .95$. The connectivity estimates correspond to rate constants and are expressed in units of 1/s (Hz). The grey lines with arrows depict intrinsic connections, with significant connections and corresponding parameter values shown in dark gray. The red/blue lines represent a positive/negative connection significantly modulated by the conditions. The mean modulatory parameter values are depicted in red for positive influence and in blue for negative influence. * denotes $p < .05$, ** $p < .01$, *** $p < .001$, and n.s. non-significant.(For interpretation of the references to color in this figure legend, the reader is referred to the web version of this article.).

Importantly, the aHPC positively influenced the TPJ (red) when the target was present in Old-All displays (Phase 1), indicative of learnt context-target associations facilitating attentional deployment to the target. However, when the target was absent, the direction was reversed: the TPJ exerted a positive influence on the aHPC, possibly reflecting the need for the updating memory-based expectations to accommodate the absence of the predicted target. No significant effects were found for New displays in Phase 1. In Phase 2, the pHPC positively influenced the TPJ (red), but only when the target was absent in Old-D displays. Assuming that pHPC holds distractor-distractor associations, its positive influence on the TPJ may indicate facilitated attentional processing due to signaling that locations usually occupied by distractors are unlikely to contain the target and thus can be ignored. In contrast, for New displays where a target was present, the pHPC impacted the TPJ (blue) negatively, down-modulating the influence of context memory on target selection. Similar to Phase 1, when expectations were violated by the target appearing at a novel location in a previously predictive context (Old-D, target present) or when the context was entirely novel and did thus not conform with any established expectations (New 2, target present or absent), the TPJ exerted a positive influence on the pHPC – suggestive of processes of mnemonic updating to accommodate the deviant target location or the newly encountered distractor arrangement.

Based on the univariate and DCM analyses, we also conducted a correlation-based MVPA in the three ROIs—the left aHPC, left pHPC, and left TPJ—as reported in the Supplementary Materials. These analyses yielded results that were supportive and complementary to the main findings.

Table 1
Activated regions in the key contrasts.

Contrast	Brain region	Cluster size (voxels)	T-value	MNI coordinates		
				x	y	z
Old-All > New1 (Target present)	L Precuneus	282	5250	−6	−55	29
	L Angular Gyrus	199	4760	−51	−64	38
	R Angular Gyrus	80	4195	45	−58	29
	L ACC	304	4662	−3	41	2
	L Superior Frontal Gyrus	231	3687	−15	44	29
	L Hippocampus	31	3813	−30	−10	−16
Old-*D* > New2	L Hippocampus	70	−3951	−21	−43	11
	R Hippocampus	67	−3919	24	−43	11
Context × Target presence	L Superior Frontal Gyrus	346	5215	−15	47	35
	L Precuneus	112	5102	−6	−55	29
	L Angular Gyrus	128	4687	−39	−61	35
	R IFG	229	−4790	45	11	26

4. Discussion

The present study investigated how the brain flexibly adapts to conditions of varying contextual predictivity during visual search. Participants first acquired and consolidated distractor-target spatial associations during training outside the scanner and continued this learning through scanning Phase 1, where both target and distractor locations were consistently repeated (target-fixed condition). This produced a classic contextual-cueing effect, with faster reaction times and higher accuracies for full-repeated compared to novel displays. Disrupting target-location predictability in scanning Phase 2 impaired both accuracy and reaction time, yet repeated distractor contexts still facilitated visual search (less than in Phase 1, but significantly relative to the baseline of novel contexts) – suggesting that contextual (re-)learning enabled efficient 'ignoring' of the distractor locations when they no longer predicted target position. These behavioral results replicate the findings of Chen and colleagues (2024, 2025a, 2005b), supporting the existence of two distinct context-based learning processes: *contextual guidance* when the distractor arrangement reliably predicts the target location, and *contextual suppression* when that arrangement becomes non-predictive. Although non-predictive contexts cannot directly guide attention to the target, they nevertheless raise the target's selection priority by down-weighting the distractor locations. The fMRI results further strengthened this distinction. Both types of memory were decoded from the hippocampus: associations linking target location with distractor context, and association binding distractor locations among themselves. Further, whole-brain univariate analysis revealed distinct anterior and posterior hippocampal regions supporting context-target and distractor-distractor learning, respectively. These (anterior, posterior) hippocampal subregions interact dynamically with the TPJ, with connectivity patterns selectively modulated by the target presence or absence depending on whether the distractor arrangement predicts the target location.

The hippocampus (HPC) has been shown to be involved in the long-term encoding and retrieval of spatial context-target associations (e.g., Eichenbaum, 2004; O'Reilly and McClelland, 1994), extending beyond its traditional role in declarative memory (e.g., Squire, 2004). For example, individuals with bilateral hippocampal damage or broader medial temporal lobe lesions exhibit impaired statistical learning, failing to extract temporal and spatial regularities from sensory input (e.g., Schapiro et al., 2014; Chun and Phelps, 1999). The hippocampus is engaged during implicit learning of repeated stimulus sequences (e.g., Rose et al., 2011), with hippocampal theta-band activity correlating with the learning of familiar contexts (Spaak and de Lange, 2020). Supporting this, Schapiro et al. (2012) used fMRI pattern similarity analyses to show that neural representations of items consistently paired within continuous sequences become more similar in the hippocampus, reflecting the extraction of shared structural features. Our findings extend this growing body of work to examine information representation in the human hippocampus (e.g., Baldassano et al., 2017; Libby et al., 2014; Ekman et al., 2023). The correlation-based MVPA results provide novel evidence that hippocampal activity patterns represent not only context-target associations but also distractor-distractor configural memory. During early phases of the task – when both the target and distractor locations repeated consistently – the hippocampus formed strong, reliable representations of the context-target relations. This robustness likely reflects extensive acquisition and consolidation of these associations, allowing the hippocampus to encode spatial-contextual maps integrating both distractor and target information. Remarkably, when target-location predictability later dissolved in Phase 2, these hippocampal representations persisted. The hippocampus continued to exhibit stable, coherent neural patterns corresponding to the old distractor-only configurations, despite their reduced predictivity for target locations.

In line with the correlation-based MVPA results, whole-brain univariate analyses showed different hippocampal subregions activated for Old versus New contexts across the two phases. The left anterior hippocampus (aHPC) activated only when a target appeared at a specific location predicted by the repeatedly encountered context-target arrangement. In contrast, bilateral posterior hippocampus (pHPC) showed stronger responses to Old versus. New contexts regardless of target presence once contextual predictivity for the target location dissolved. These results were further supported by the correlation-based MVPA to these regions (see **Fig. S1** in the Supplementary Materials). Within the context–target association–related aHPC, higher similarity for Old compared with New displays during Phase 1 indicated well-established context–target associations prior to scanning. Notably, the absence of a significant difference between Old-present and Old-absent displays in this phase suggests that these two conditions evoked highly similar representations, consistent with a shared context–target associative code. In the context-related pHPC, Old displays consistently showed higher similarity than New displays. Importantly, the absence of a difference between Old-present and Old-absent displays in Phase 2 (rather than Phase 1) indicates that the pHPC maintained similar context-based representations after losing predictive value.

This finding aligns with established *functional dissociation* along the hippocampal longitudinal axis (Stokes et al. 2015): the aHPC forms and encodes associative or global representations, engaging more during initial learning than later retrieval (Kim, 2015; Poppenk et al., 2013), whereas the pHPC retrieves detailed, context-rich memories (Kim, 2015; Poppenk et al., 2013). Recent model-based representational similarity analyses during navigation in realistic virtual environments showed that the aHPC encodes larger predictive horizons than the pHPC (Brunec and Momennejad, 2022), converging with our findings and supporting a functional gradient along the hippocampal long axis. The convergence between correlation-based MVPA and whole-brain univariate analyses demonstrates that qualitatively different fMRI methodologies can provide complementary evidence on underlying representations, highlighting the synergistic potential of combining encoding and decoding approaches to better understand the neural basis of statistical learning in visual search.

Beyond the hippocampus, our findings position the TPJ as a key node in supporting efficient visual search by leveraging long-term contextual memory. While traditionally linked to stimulus-driven attentional reorienting (Corbetta and Shulman, 2002), our results align with the TPJ also mediating attention allocation based on internal memory signals (Geng and Vossel, 2013; Cabeza et al., 2008). Specifically, TPJ tracks

hippocampal signals reflecting prioritized locations derived from statistical learning. This attentional read-out of memory content likely enables rapid guidance toward learnt target locations or reduces attentional processing of distractors when target locations become unpredictable. This pattern emerged in increased TPJ activation for fully repeated (vs. new) displays with predictable target locations and reduced TPJ activity on target-absent trials for learnt contexts that had lost target-location predictivity. These findings suggest TPJ supports multiple attentional functions: direct target-location prioritization through contextual guidance (i.e., 'contextual cueing' in the proper sense) with fully predictive distractor arrangements, and relative prioritization of target over distractor locations via distractor-context suppression with non-predictive arrangements. Since the target location becomes unbound from the context, down-weighting the distractors as a group indirectly raises the priority of the target.

The dynamic nature of TPJ-HPC connectivity further suggests that these regions flexibly interact depending on the predictivity of the visual context with respect to the target location. TPJ tracks both target-related memory representations (e.g., target-context associations) and non-target contextual representations (e.g., distractor-distractor bindings) – consistent with an interpretation of its role in context-based visual search within a predictive-coding framework. When target-context associations were reliable (Old-All), the aHPC positively influenced the TPJ, supporting memory-guided attentional orienting directly to the predicted target location. When the target was absent in a less predictive but familiar context (Old-D), the pHPC also exerted a positive influence on TPJ, likely facilitating the down-weighting, or 'suppression', of distractor locations based on sole-context (re-)learning, thus indirectly raising the selection priority assigned to the target location. However, the direction of influence reversed when contextual predictions were either unconfirmed on trials of target absence after reliable context-target association learning, or when they were downright violated by the target appearing at an unexpected location in Old-D displays, or when novel contexts not matching any established memory representation were encountered: in all these cases, TPJ positively influenced the pHPC, suggesting a shift toward mnemonic updating in response to 'unusual' input. Additionally, for New displays with target presence, the pHPC also negatively influenced the TPJ, indicating reduced reliance on contextual memory under conditions of contextual novelty and unpredictability. Thus, TPJ contributes not only to detecting memory-based attentional signals, but also to adaptively coordinating memory and attention systems in a flexible, context-sensitive manner. These findings parallel those of Isenburg et al. (2023), who showed long-term-memory-guided attention to involve flexible network-level reconfiguration: hippocampal regions (a default-mode node) increased connectivity with dorsal attention areas when attention was guided by memory. Our observed HPC-TPJ coupling reflects a more localized version of this broader pattern: memory output from the HPC positively influences TPJ to directly guide target selection or indirectly suppress distractors based on prior context-target association or sole-context learning. Our results demonstrate that such HPC-TPJ interactions can occur even without explicit awareness, extending previous findings from episodic memory studies to the domain of implicit statistical learning. The dynamic interaction between hippocampus and TPJ underscores how predictive and non-predictive learning engage distinct yet complementary neural pathways to optimize visual search performance.

Our findings support two distinct forms of contextual learning: contextual guidance when repeated distractor arrangements reliably predict the target location, and contextual down-weighting when the target position varies unpredictably relative to familiar distractor configurations. In the latter case, the observed modulation of hippocampal and TPJ activity may reflect adaptive suppression of previously predictive contextual information that has become unreliable. Nevertheless, alternative mechanisms warrant consideration. One possibility is that these effects arise from expectation violation or mismatch detection, whereby the hippocampus signals that an established context no longer predicts the target, leading to reduced reactivation of the learned association. Another possibility is reduced retrieval or re-engagement of context representations once they lose behaviorally relevant, rather than active suppression per se. Distinguishing between these accounts will require further neuroimaging work using paradigms specifically designed to dissociate context suppression, expectation violation, and retrieval disengagement processes.

5. Conclusion

Our findings support the notion of two distinct forms of contextual learning: contextual guidance, when repeated distractor arrangements reliably predict the respective target location, and distractor suppression, when the target position varies unpredictably relative to the distractor configuration. Both context-target and distractor–distractor spatial associations are decodable from the hippocampus, with whole-brain univariate analyses revealing a division of labor between anterior and posterior hippocampal regions. These anatomically distinct hippocampal circuits encode the different types of spatial regularity, while the TPJ dynamically gates their influence on attentional processing depending on the predictivity of the context.

Code and data accessibility

The data and key analysis code supporting the study's findings are available at https://gin.g-node.org/siyi.chen/CCfMRI. This study's design and its analysis were not preregistered.

CRediT authorship contribution statement

Siyi Chen: Writing – original draft, Visualization, Project administration, Methodology, Investigation, Funding acquisition, Formal analysis, Data curation, Conceptualization. **Si Cheng:** Software, Investigation. **Thomas Geyer:** Writing – review & editing, Methodology, Conceptualization. **Hermann J. Müller:** Writing – review & editing, Validation, Methodology, Conceptualization. **Zhuanghua Shi:** Writing – review & editing, Resources, Project administration, Methodology, Funding acquisition, Conceptualization.

Declaration of competing interest

The authors declare no competing financial interests.

Acknowledgments

This work was supported by German Research Foundation (DFG; Deutsche Forschungsgemeinschaft) grants CH 3093/1-1 and SH 166/10-1, awarded to SC and ZS, respectively, and was done using the NICUM Siemens Prisma scanner supported by DFG grant INST 86/1739-1 FUGG.

Supplementary materials

Supplementary material associated with this article can be found, in the online version, at doi:10.1016/j.neuroimage.2025.121582.

References

Awh, E., Belopolsky, A.V., Theeuwes, J., 2012. Top-down versus bottom-up attentional control: a failed theoretical dichotomy. Trends. Cogn. Sci. 16, 437–443. https://doi.org/10.1016/j.tics.2012.06.010. Available at:

Baldassano, C., Chen, J., Zadbood, A., Pillow, J.W., Hasson, U., Norman, K.A., 2017. Discovering event structure in continuous narrative perception and memory. Neuron 95, 709–721. https://doi.org/10.1016/j.neuron.2017.06.041 e5 Available at:

Brainard, D.H., 1997. The psychophysics toolbox. Spat. Vis. 10, 433–436. https://doi.org/10.1163/156856897x00357. Available at:

Brooks, M.E., Kristensen, K., Van Benthem, K.J., 2017. glmmTMB balances speed and flexibility among packages for zero-inflated generalized linear mixed modeling. R J. 9, 378–400. https://doi.org/10.32614/RJ-2017-066. Available at:

Brunec, I.K., Momennejad, I., 2022. Predictive representations in hippocampal and prefrontal hierarchies. J. Neurosci. 42, 299–312. https://doi.org/10.1523/JNEUROSCI.1327-21.2021. Available at:
Cabeza, R., Ciaramelli, E., Olson, I.R., Moscovitch, M., 2008. The parietal cortex and episodic memory: an attentional account. Nat. Rev. Neurosci. 9, 613–625. https://doi.org/10.1038/nrn2459. Available at:
Chen, S., Müller, H.J., Shi, Z., 2024. Contextual facilitation: separable roles of contextual guidance and context suppression in visual search. Psychon. Bull. Rev. https://doi.org/10.3758/s13423-024-02508-1. Available at:
Chen, S., Allenmark, F., Merkuš, N., Müller, H.J., Shi, Z., 2025a. Context-based guidance versus context suppression in contextual learning: role of un-/certainty in the target-context relations in visual search. J. Exp. Psychol. Hum. Percept. Perform. https://doi.org/10.1037/xhp0001321. Available at:
Chen, S., Merkuš, N., Tsai, S.Y., Cheng, S., Müller, H.J., Shi, Z., 2025b. Statistical context learning in visual search: distinct electrophysiological signatures of contextual guidance and context suppression. J. Neurosci. 45. https://doi.org/10.1523/JNEUROSCI.2186-24.2025. Available at:
Chun, M.M., Jiang, Y., 1998. Contextual cueing: implicit learning and memory of visual context guides spatial attention. Cogn. Psychol. 36, 28–71. https://doi.org/10.1006/cogp.1998.0681. Available at:
Chun, M.M., Nakayama, K., 2000. On the functional role of implicit visual memory for the adaptive deployment of attention across scenes. Vis. cogn. 7, 65–81. https://doi.org/10.1080/135062800394685. Available at:
Chun, M.M., Phelps, E.A., 1999. Memory deficits for implicit contextual information in amnesic subjects with hippocampal damage. Nat. Neurosci. 2, 844–847. https://doi.org/10.1038/12222. Available at:
Corbetta, M., Shulman, G.L., 2002. Control of goal-directed and stimulus-driven attention in the brain. Nat. Rev. Neurosci. 3, 201–215. https://doi.org/10.1038/nrn755. Available at:
Dugué, L., Merriam, E., Heeger, D., Carrasco, M., 2018. Specific visual subregions of TPJ mediate reorienting of spatial attention. Cereb. Cortex 28, 2375–2390. https://doi.org/10.1093/cercor/bhx140. Available at:
Eichenbaum, H., 2004. Hippocampus: cognitive maps or relational memory? Nat. Rev. Neurosci. 5 (11), 30–40. https://doi.org/10.1038/nrn1489.
Ekman, M., Kusch, S., de Lange, F.P., 2023. Successor-like representation guides the prediction of future events in human visual cortex and hippocampus. Elife 12. https://doi.org/10.7554/eLife.78904. Available at:
Friston, K.J., Penny, W., 2011. Post hoc bayesian model selection. Neuroimage 56, 2089–2099. https://doi.org/10.1016/j.neuroimage.2011.03.062.
Friston, K.J., Harrison, L., Penny, W., 2003. Dynamic causal modeling. Neuroimage 19 (4), 1273–1302. https://doi.org/10.1016/S1053-8119(03)00202-7.
Friston, K.J., Litvak, V., Oswal, A., Razi, A., Stephan, K.E., van Wijk, B.C.M., Ziegler, G., Zeidman, P., 2016. Bayesian model reduction and empirical Bayes for group (DCM) studies. Neuroimage 128, 413–431. https://doi.org/10.1016/j.neuroimage.2015.11.015.
Friston, K., 2005. A theory of cortical responses. Philos. Trans. R. Soc. Lond. B Biol. Sci. 360, 815–836. https://doi.org/10.1098/rstb.2005.1622. Available at:
Friston, K., 2008. Hierarchical models in the brain. PLoS. Comput. Biol. 4, e1000211. https://doi.org/10.1371/journal.pcbi.1000211. Available at:
Geng, J.J., Behrmann, M., 2005. Spatial probability as an attentional cue in visual search. Percept. Psychophys. 67, 1252–1268. https://doi.org/10.3758/bf03193557. Available at:
Geng, J.J., Mangun, G.R., 2011. Right temporoparietal junction activation by a salient contextual cue facilitates target discrimination. Neuroimage 54, 594–601. https://doi.org/10.1016/j.neuroimage.2010.08.025. Available at:
Geng JJ, Vossel S (2013) Re-evaluating the role of TPJ in attentional control: contextual updating? Neurosci Biobehav Rev 37:2608–2620 Available at: https://doi.org/10.1016/j.neubiorev.2013.08.010.
Geyer, T., Baumgartner, F., Müller, H.J., Pollmann, S., 2012. Medial temporal lobe-dependent repetition suppression and enhancement due to implicit vs. explicit processing of individual repeated search displays. Front. Hum. Neurosci. 6. https://doi.org/10.3389/fnhum.2012.00272. Available at:
Giesbrecht B, Sy JL, Guerin SA (2013) Both memory and attention systems contribute to visual search for targets cued by implicitly learned context. Vision Res 85:80–89 Available at: https://doi.org/10.1016/j.visres.2012.10.006.
Goujon, A., Didierjean, A., Thorpe, S., 2015. Investigating implicit statistical learning mechanisms through contextual cueing. Trends. Cogn. Sci. 19, 524–533. https://doi.org/10.1016/j.tics.2015.07.009. Available at:
Grahn, J.A., Parkinson, J.A., Owen, A.M., 2008. The cognitive functions of the caudate nucleus. Prog. Neurobiol. 86, 141–155. https://doi.org/10.1016/j.pneurobio.2008.09.004. Available at:
Green, DM, Swets, JA, 1966. Others. In: Signal detection theory and psychophysics. Wiley, New York.
Greene, A.J., Gross, W.L., Elsinger, C.L., Rao, S.M., 2007. Hippocampal differentiation without recognition: an fMRI analysis of the contextual cueing task. Learn. Mem. 14, 548–553. https://doi.org/10.1101/lm.609807. Available at:
Grill-Spector, K., Henson, R., Martin, A., 2006. Repetition and the brain: neural models of stimulus-specific effects. Trends. Cogn. Sci. 10, 14–23. https://doi.org/10.1016/j.tics.2005.11.006. Available at:
Haxby, J.V., Gobbini, M.I., Furey, M.L., Ishai, A., Schouten, J.L., Pietrini, P., 2001. Distributed and overlapping representations of faces and objects in ventral temporal cortex. Science 293, 2425–2430. https://doi.org/10.1126/science.1063736. Available at:
Hebart, M.N., Görgen, K., Haynes, J.-D., 2014. The decoding Toolbox (TDT): a versatile software package for multivariate analyses of functional imaging data. Front. Neuroinform. 8, 88. https://doi.org/10.3389/fninf.2014.00088. Available at:
Isenburg, K., Morin, T.M., Rosen, M.L., Somers, D.C., Stern, C.E., 2023. Functional network reconfiguration supporting memory-guided attention. Cerebr. Cortex 33, 7702–7713. https://doi.org/10.1093/cercor/bhad073. Available at:
Kim, H., 2015. Encoding and retrieval along the long axis of the hippocampus and their relationships with dorsal attention and default mode networks: the HERNET model: encoding and retrieval along the long axis. Hippocampus 25, 500–510. https://doi.org/10.1002/hipo.22387. Available at:
Libby, L.A., Hannula, D.E., Ranganath, C., 2014. Medial temporal lobe coding of item and spatial information during relational binding in working memory. J. Neurosci. 34, 14233–14242. https://doi.org/10.1523/JNEUROSCI.0655-14.2014. Available at:
Manelis A, Reder LM (2012) Procedural learning and associative memory mechanisms contribute to contextual cueing: Evidence from fMRI and eye-tracking. Learn Mem 19:527–534 Available at: https://doi.org/10.1101/lm.025973.112.
Manginelli, A.A., Baumgartner, F., Pollmann, S., 2013. Dorsal and ventral working memory-related brain areas support distinct processes in contextual cueing. Neuroimage 67, 363–374. https://doi.org/10.1016/j.neuroimage.2012.11.025. Available at:
O'Reilly, R.C., McClelland, J.L., 1994. Hippocampal conjunctive encoding, storage, and recall: avoiding a trade-off. Hippocampus 4, 661–682. https://doi.org/10.1002/hipo.450040605. Available at:
Packard, M.G., Knowlton, B.J., 2002. Learning and memory functions of the Basal Ganglia. Annu. Rev. Neurosci. 25, 563–593. https://doi.org/10.1146/annurev.neuro.25.112701.142937. Available at:
Pelli, D.G., 1997. The VideoToolbox software for visual psychophysics: transforming numbers into movies. Spat. Vis. 10, 437–442. https://doi.org/10.1163/156856897X00366. Available at:
Penny, W., Mattout, J., Trujillo-Barreto, N., 2006. Bayesian model selection and averaging. Statistical Parametric Mapping: the Analysis of Functional Brain Images. Elsevier, London.
Pollmann S, Manginelli AA (2010) Repeated Contextual Search Cues Lead to Reduced BOLD-Onset Times in Early Visual and Left Inferior Frontal Cortex. Open Neuroimag J 4:9–15 Available at: https://doi.org/10.2174/1874440001004010009.
Poppenk, J., Evensmoen, H.R., Moscovitch, M., Nadel, L., 2013. Long-axis specialization of the human hippocampus. Trends. Cogn. Sci. 17 (5), 230–240. https://doi.org/10.1016/j.tics.2013.03.005.
Preston, A.R., Gabrieli, J.D.E., 2008. Dissociation between explicit memory and configural memory in the human medial temporal lobe. Cereb. Cortex 18, 2192–2207. https://doi.org/10.1093/cercor/bhm245. Available at:
Rose, M., Haider, H., Salari, N., Büchel, C., 2011. Functional dissociation of hippocampal mechanism during implicit learning based on the domain of associations. J. Neurosci. 31, 13739–13745. https://doi.org/10.1523/JNEUROSCI.3020-11.2011. Available at:
Schapiro, A.C., Kustner, L.V., Turk-Browne, N.B., 2012. Shaping of object representations in the human medial temporal lobe based on temporal regularities. Curr. Biol. 22, 1622–1627. https://doi.org/10.1016/j.cub.2012.06.056. Available at:
Schapiro, A.C., Gregory, E., Landau, B., McCloskey, M., Turk-Browne, N.B., 2014. The necessity of the medial temporal lobe for statistical learning. J. Cogn. Neurosci. 26, 1736–1747. https://doi.org/10.1162/jocn_a_00578. Available at:
Shulman, G.L., McAvoy, M.P., Cowan, M.C., Astafiev, S.V., Tansy, A.P., d'Avossa, G., Corbetta, M., 2003. Quantitative analysis of attention and detection signals during visual search. J. Neurophysiol. 90, 3384–3397. https://doi.org/10.1152/jn.00343.2003. Available at:
Shulman, G.L., Astafiev, S.V., McAvoy, M.P., d'Avossa, G., Corbetta, M., 2007. Right TPJ deactivation during visual search: functional significance and support for a filter hypothesis. Cereb. Cortex 17, 2625–2633. https://doi.org/10.1093/cercor/bhl170. Available at:
Spaak, E., de Lange, F.P., 2020. Hippocampal and prefrontal theta-band mechanisms underpin implicit spatial context learning. J. Neurosci. 40, 191–202. https://doi.org/10.1523/JNEUROSCI.1660-19.2019. Available at:
Squire, L.R., 2004. Memory systems of the brain: a brief history and current perspective. Neurobiol. Learn. Mem. 82, 171–177. https://doi.org/10.1016/j.nlm.2004.06.005. Available at:
Stokes, J., Kyle, C., Ekstrom, A.D., 2015. Complementary roles of human hippocampal subfields in differentiation and integration of spatial context. J. Cogn. Neurosci. 27, 546–559. https://doi.org/10.1162/jocn_a_00736. Available at:
Summerfield, C., Trittschuh, E.H., Monti, J.M., Mesulam, M.M., Egner, T., 2008. Neural repetition suppression reflects fulfilled perceptual expectations. Nat. Neurosci. 11, 1004–1006. https://doi.org/10.1038/nn.2163. Available at:
Vadillo, M.A., Giménez-Fernández, T., Beesley, T., Shanks, D.R., Luque, D., 2021. There is more to contextual cuing than meets the eye: improving visual search without attentional guidance toward predictable target locations. J. Exp. Psychol. Hum. Percept. Perform. 47, 116–120. https://doi.org/10.1037/xhp0000780. Available at:
Wei, P., Müller, H.J., Pollmann, S., Zhou, X., 2009. Neural basis of interaction between target presence and display homogeneity in visual search: an fMRI study. Neuroimage 45, 993–1001. https://doi.org/10.1016/j.neuroimage.2008.12.053. Available at:
Westerberg, C.E., Miller, B.B., Reber, P.J., Cohen, N.J., Paller, K.A., 2011. Neural correlates of contextual cueing are modulated by explicit learning. Neuropsychologia 49, 3439–3447. https://doi.org/10.1016/j.neuropsychologia.2011.08.019. Available at: